Continuous Hidden Markov Model for Pedestrian Activity Classification and Gait Analysis

Ghazaleh Panahandeh*, *Student Member, IEEE,* Nasser Mohammadiha, *Student Member, IEEE,* Arne Leijon, *Member, IEEE,* and Peter Händel, *Senior Member, IEEE*

Abstract

This paper presents a method for pedestrian activity classification and gait analysis based on the MEMS inertial measurement unit (IMU). The work targets two groups of applications including 1) human activity classification and 2) joint human activity and gait-phase classification. In the latter case, the gait-phase is defined as a sub-state of a specific gait cycle, i.e., the states of the body between the stance and swing phases. We model the pedestrian motion with a continuous hidden Markov model (HMM) in which the output density functions are assumed to be Gaussian mixture models (GMMs). For the joint activity and gait-phase classification, motivated by the cyclical nature of the IMU measurements, each individual activity is modeled by a "circular HMM". For both the proposed classification methods, proper feature vectors are extracted from the IMU measurements. In the present work, we report the results of conducted experiments where the IMU was mounted on the humans' chests. This permits the potential application of the current study in camera-aided inertial navigation for positioning and personal assistance for future research works. Five classes of activity including: walking, running, going upstairs, going downstairs, and standing are considered in the experiments. The performance of the proposed methods is illustrated in various ways, and as an objective measure, the confusion matrix is computed and reported. The achieved relative figure-of-merits using the collected data validates the reliability of the proposed methods for the desired applications.

Index Terms

Inertial measurement unit, activity classification, gait analysis, hidden Markov model.

I. Introduction

Recently, considerable research within the instrumentation and measurement community has been devoted to the application of micro-electromechanical system (MEMS) inertial sensors in different areas such as inertial navigation [1], [2], [3], vehicle applications [4], [5], behavioral analysis [6], and biomedical applications [7], [8]. This is mainly motivated by the development of the MEMS technology to provide such a lightweight and cheap motion capture sensor, which is becoming a standard feature of smart-phones and personal digital assistants.

The authors are with the School of Electrical Engineering, ACCESS Linnaeus Centre, KTH Royal Institute of Technology, SE-10044 Stockholm, Sweden. email: {ghpa, nmoh, leijon, ph}@kth.se

Hence, MEMS inertial measurement units (IMUs) can be considered as fundamental and primary motion capture sensors. IMU sensors have been successfully used in human locomotion analysis such as human activity monitoring, gesture recognition, fall detection, balance control evaluation, and abnormal behavior detection [9], [10], [11], [12], [13]. Another widely investigated application of IMU is in inertial navigation systems, which has recently received increasing attention in the instrumentation and measurement community, e.g., personal navigation and dead-reckoning [14], [15], [16], and road vehicle navigation [17].

IMU-based positioning systems, however, suffer from integration drift; small errors in the measurement of acceleration and angular velocity are integrated into progressively larger errors in velocity, which are compounded into still greater errors in position. Therefore, the estimated pose must be periodically corrected by additional information. This information can either be provided by an additional sensor such as a GPS [18], [19], [20] and camera [1], [21], or an algorithm that intelligently takes into account the state of the system, e.g., zero velocity update (ZUPT) in foot-mounted IMU pedestrian navigation [14], [22], [23]. However, in the commonly used threshold-based ZUPT methods, integrating activity classification and dead reckoning techniques can lead to a better choice for the threshold value and therefore, can improve the performance of the navigation system [24], [25]. Apart from the foot-mounted IMU, pedestrian vision-aided inertial navigation systems can be counted among the most reliable positioning systems if the activity-type of the moving subjects can be integrated with the image data (to avoid motion blurred images and provide step information) [1], [26].

Human activity classification is also an important aspect of diseases diagnosis and assistance health care in medical centers; with for instance, early fall detection to rescue subjects [27], [28] and metabolic energy expenditure [13], [29]. In addition to the activity classification, reliable gait-phase classification is an important topic for human locomotion analysis and identifying abnormality [7], [8], [30]. Moreover, the referred step information in the two mentioned positioning systems is closely related to the gait analysis. Gait analysis involves the recognition of the underlying gait-phases; a gait-phase is defined as a state of the body during the stance and swing phases of each step while walking, running, etc. Among the gait-phase classification methods, we can refer to threshold-based approaches [30], [31] and fuzzy logic methods [8] in which the system must be individually calibrated for different users.

The current activity and gait-phase classifications methods, however, suffer from a lack of robustness, e.g., they are threshold-based [30], [31], have to be calibrated for different individuals [8], or are not suitable for vision-aided inertial navigation systems because they are developed for foot-mounted IMU [24]. Moreover, the joint activity and gait-phase classification has not been fully considered in the available literature.

The main contribution of the current study is to develop a probabilistic, user-independent approach for activity and gait-phase classification using an upper-body positioned IMU, specifically, chest-mounted IMU (Chem-IMU);

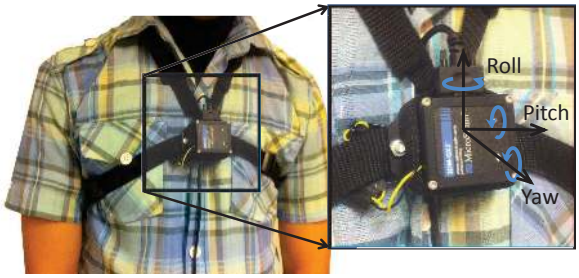

Fig. 1: Illustration of chest-mounted IMU (Chem-IMU). The black box indicates the IMU sensor mounted on the chest of a sample participant. The drawing axes on the IMU illustrate approximately the direction of the accelerometers and gyroscopes' measurements.

see Fig. 1. The upper-body positioned IMU experiences less vibration and noise during movement compared to the lower-body positioned IMU [32]; additionally, it provides a wide field of view for a camera to be used in the vision-aided inertial navigation systems [1], [21], [26], [33], [34].

The proposed novel classification methods are based on the hidden Markov model (HMM). In this application, the hidden states are in fact different activity classes or gait phases. Since the IMU measurements are usually quantized with a large number of bits, we propose using a continuous HMM (HMM with continuous output density functions) rather than a discrete HMM as in [10], [35], [36]. The state-conditional output density functions of HMM are assumed to be a Gaussian mixture model (GMM) that is powerful in modeling any continuous distribution desired. We propose two HMM-based solutions for 1) activity classification, and 2) joint activity and gait-phase classification. The proposed activity classification is based on the method introduced in [37]. The joint activity and gait-phase classification is achieved via the modeling of IMU measurements within each activity-type using a circular HMM. Given that no other algorithm is proposed in the literature for the considered Chem-IMU setup (to the best of our knowledge), the performance of the proposed classification techniques is self-analyzed, and the correct classification rate is calculated as the relative figure-of-merit. The achieved promising results verify the merit of the proposed algorithms for the desired applications.

The paper is organized as follows: the measurement and sensor model is described in Section II, the problem description and the proposed classification methods are presented in Section III, experimental validation is reported in Section IV, discussion is given in Section V and finally, the conclusion of the study is summarized in Section VI.

II. Measurement and Sensor Model

The classification of pedestrian activity is achieved by using the measurements from the three orthogonal gyroscopes and the three orthogonal accelerometer clusters of the IMU. A MicroStrain 3DM-GX2 IMU was used in the experiments. This converts the motion sensors' raw voltage outputs into a digital format (in terms of A/D converter codes) with a sampling rate of 250 Hz. The accelerometer measurements are then re-scaled into physical

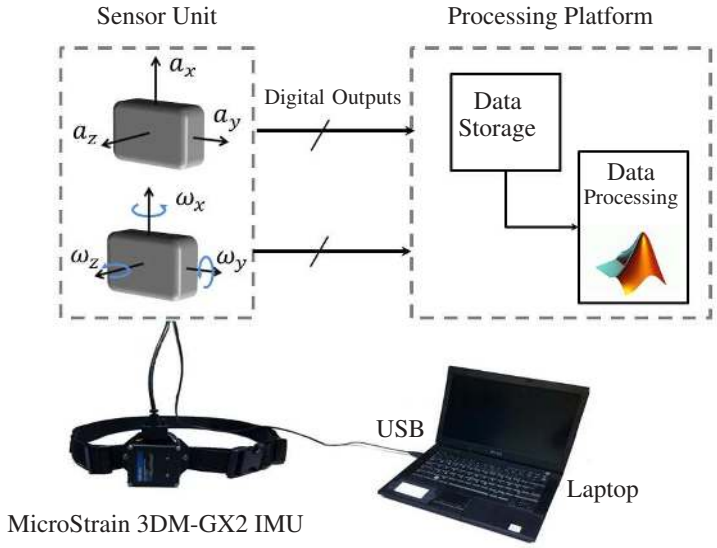

Fig. 2: Overall system architecture. The sensor module, considered to be an IMU, consists of three orthogonal accelerometers and three orthogonal gyroscopes. The stored IMU measurements are processed by a laptop to perform the classification. This occurs in the processing platform.

units of g ($1\ g = 9.80665\ m/s^2$). Independent of the IMU's position, the measurements of the accelerometer, $\mathbf{a}_k \in \mathbb{R}^3$, and the gyroscope, $\omega_k \in \mathbb{R}^3$, clusters of the IMU, Fig. 2, are modeled as:

$$\mathbf{y}_k = \mathbf{x}_k + \mathbf{n}_k \in \mathbb{R}^6, \tag{1}$$

where

$$\mathbf{x}_k = \begin{bmatrix} \mathbf{a}_k \\ \omega_k \end{bmatrix}, \qquad \text{and} \qquad \mathbf{n}_k = \begin{bmatrix} \mathbf{n}_k^{\mathbf{a}} \\ \mathbf{n}_k^{\omega} \end{bmatrix},$$

$\mathbf{n}_k^{\mathbf{a}} \in \mathbb{R}^3$ and $\mathbf{n}_k^{\omega} \in \mathbb{R}^3$ are noise vectors associated with the acceleration and angular rates, respectively. k is the corresponding sample index.

For the data collection, users were asked to connect the IMU to their chest, with no particular consideration to the IMU placement, as illustrated in Fig. 1. It should be noted that mounting the sensor in slightly different positions, on different individuals, or in different environments may cause additional noise or biases in the measurements. Moreover, due to the random nature of the additive noise, equation (1) should rather be analyzed stochastically. In the proposed methodology (Section III), these issues are recalled and are solved by applying a proper pre-processing and modeling of the signal.

Fig. 2 provides a general overview of the system architecture. The IMU sensor unit is shown on the left-hand side. The sensor module carried by the participants is directly connected to a laptop via a USB port. The IMU measurements are first stored in the processing platform, and then the classification is done off-line at MATLAB

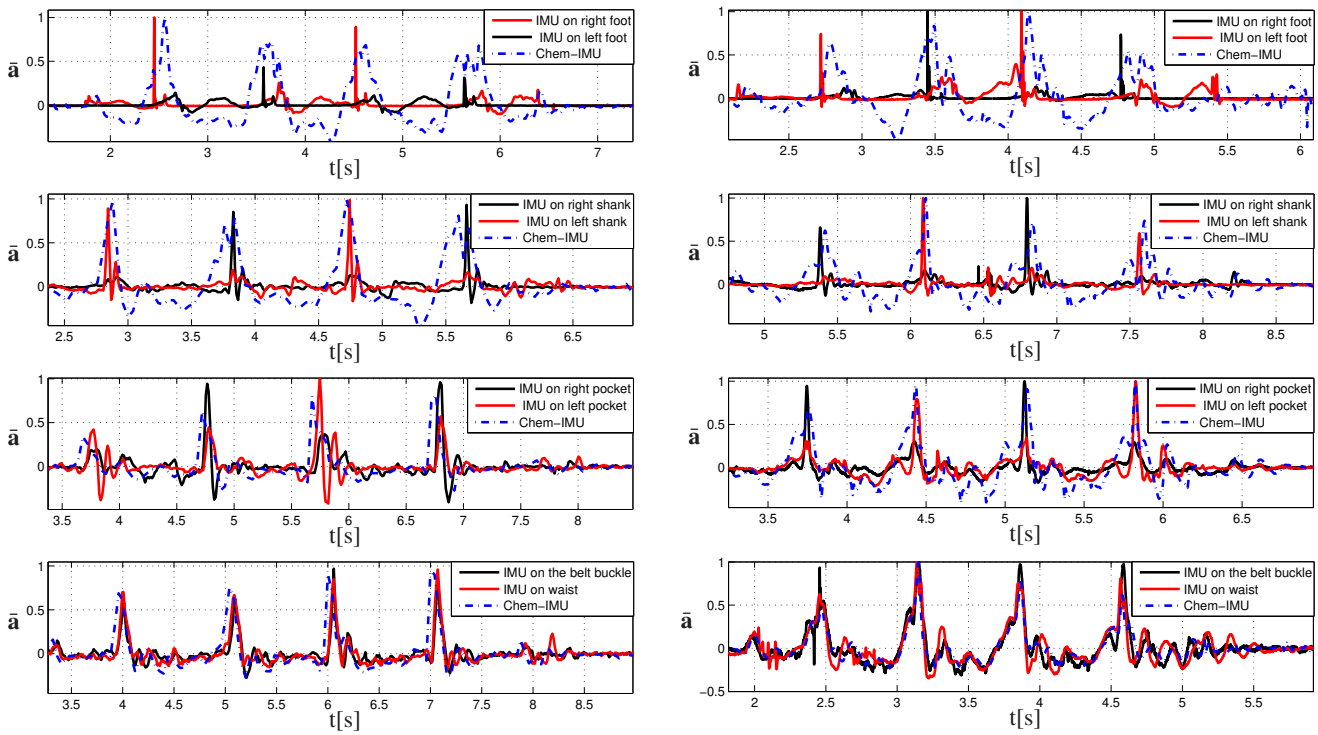

(a) First subject with height 185 cm

(b) Second subject with height 167 cm

Fig. 3: Comparison between the cyclical pattern of the Chem-IMU and the IMUs mounted on the: feet, shanks, pockets, waist (close to L3 vertebra) and belt buckle. The vertical axes indicate the normalized norm of the accelerometers' measurements $\bar{\mathbf{a}} = \frac{\|\mathbf{a}\|}{\max(\|\mathbf{a}\|)}$.

via the processing module.

Although the primary goals of this work are pedestrian activity and gait-phase classification through a wearable IMU, we are also interested in the future application of the classifier where the IMU is coupled with a secondary vision system for inertial navigation. As a result, the IMU is considered to be placed on the chest. However, the proposed methods are not restricted to the Chem-IMU setup and they can be used for different IMU placements on the human body as far as the IMU signals present a cyclical nature corresponding to the human motions. Fig. 3 represents such cyclical patterns for different IMU body placements for two sample participants. In this figure the vertical axes indicate the normalized norm of the accelerometers measurements. Four different experiments were done in which the Chem-IMU signals were compared with the measurements from IMUs placed on different parts of the subject's body as follows: feet, shanks, pockets, and finally on the waist close to the L3 vertebra and on the belt buckle. In the normal walking scenario, each step is due to the movement of one of the legs while the other leg's foot is stationary on the ground. Hence, to totally represent four steps, two IMUs were placed symmetrically on both the right and left legs, meanwhile, a single upper-body positioned IMU can provide the full representation of each step.

III. Activity and Gait-phase Classification

A. Problem Description

Walking is characterized by the cyclical movements of the lower limbs, [9], in which the stance and swing phases define each gait cycle. However, using the measurements from the IMU mounted on the other parts of the body (Fig. 3), a similar analysis can be performed to define different gait cycles. In the proposed methods, the following classes of activity are considered for classification: walking, running, going upstairs, going downstairs and standing (no rigid body acceleration). This latter state corresponds to the case when the user is standing still, however, no restriction for the rotation is considered. Represented symbolically:

$$\frac{1}{L}\sum_{k=1}^{L}\|\mathbf{a}_k\| \approx g, \tag{2}$$

where L is the length of the analysis window, g is the magnitude of the local gravity vector, and $\|\cdot\|$ indicates the norm operation. Although only five categories of the human physical activities are considered in this study, other activities such as bending, sitting down and standing up can also be considered as additional states in the proposed classification approaches.

B. Methodology

Both of the proposed methods for the activity, and joint activity and gait-phase classification consist of three steps: 1) pre-processing, 2) feature extraction, and 3) classification.

The digital pre-processing module of the system is a band-pass filter that reduces measurement noise and removes the effect of the IMU displacement on the chest for different subjects. The band-pass filter is a combination of a standard low-pass filter $f_{\text{cutoff}} = 20$ Hz) and a DC level cancelation.

To both gain a better description of the signals' characteristics and reduce the dimensions of the signal, a feature extraction method is used once the noise reduction has been applied to the IMU measurements. The extracted feature vectors should best discriminate between different patterns. Various kinds of feature extraction methods have been considered for activity classification in the literature such as vector quantization [10], principal component analysis (PCA) [38], frequency analysis [36], and time-frequency analysis [39]. A comprehensive study on the sensor-based feature extraction methods for activity classification can be found in [9], [40], [41]. Depending on the considered problem, two different types of feature extraction methods are used in this paper. The details of the feature extraction units and the classification techniques are given in the following.

1) Activity Classification: In this problem, we focus on the pedestrian activity classification in which further analysis of the underlying gait cycle (a period of the IMU measurement during each activity) is not of interest. To exploit the prior knowledge that the type of activity does not change rapidly, it is proper to use the long-term

properties of the IMU signals to recognize the activity type. Therefore, time-frequency domain (TF domain) analysis is used for the feature extraction. For human activity, the IMU measurements are assumed to be a locally stationary stochastic process within short windows up to $1 \sim 2$ seconds; that is $250 \sim 500$ samples at a 250 Hz sampling rate. Hence, we apply a discrete Fourier transform (DFT) to the signals with overlapped short-time frames. The frame length should be chosen such that the signal can be considered stationary within each frame while the overlap length influences the update frequency of the classification results. In our experiments, the frame length was chosen to be 512 samples with 75% overlap between consecutive frames. The windowing of the signal into the short-time frames was done using a Hann window rather than a rectangular window to reduce the edge effects of the windowing. Furthermore, the DFT length was chosen to be equal to the length of the short-time frames, which corresponds to a 512-point DFT in our setup. For the feature extraction, the first 10 DFT coefficients (coefficients 1 to 10) of the IMU measurements are transferred to the log-spectral domain by taking the logarithm of the magnitude-squared DFT coefficients. Then, the obtained features for each of the IMU signals are concatenated to make a 60-length vector for the current time-frame. The variances of the signals in each segment are also explicitly concatenated to these vectors to obtain the complete feature vector that is represented by $\mathbf{z}_l$ in the following (Fig. 4).

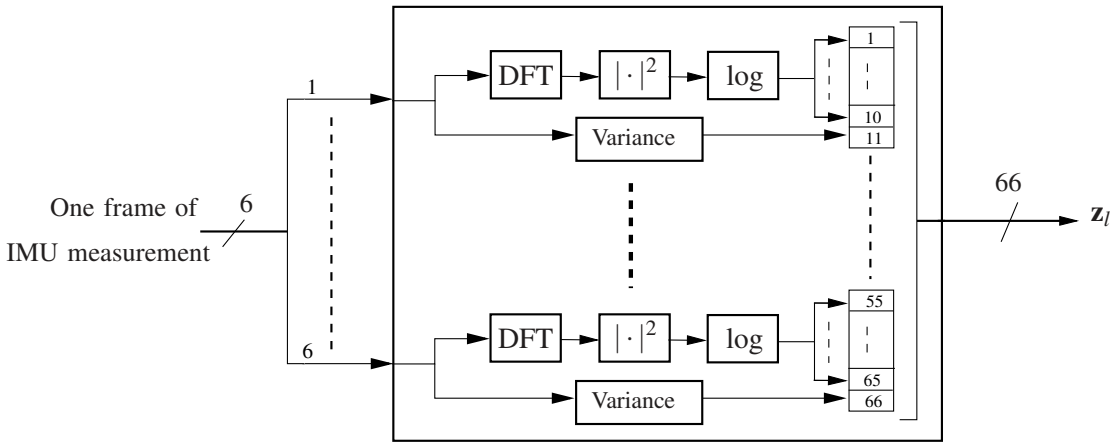

Fig. 4: Illustration of the feature vector $\mathbf{z}_l$ used for activity classification. For each segment of data, the logarithm of the magnitude-squared of the first 10 DFT coefficients and variance of the data is used to construct $\mathbf{z}_l$.

The described TF analysis implies that the classification result always has a lag that is approximately equal to the "frame length – overlap length". However, this delay is tolerable in pedestrian activity classification. In our set-up it corresponds to 128 samples. The nice property of the TF analysis is that different activities are easily discriminated based on their frequency characteristics. For instance, the usual cycle-duration of walking is around $0.5 \sim 1$ seconds meaning that the sinusoidal harmonic at $1 \sim 2$ Hz in the frequency analysis will have the highest energy. On the other hand, with running for example the sinusoidal harmonic at $4 \sim 6$ Hz will have the highest energy.

Here, the human activity is modeled with a continuous HMM using a first order Markov chain; thus, an HMM

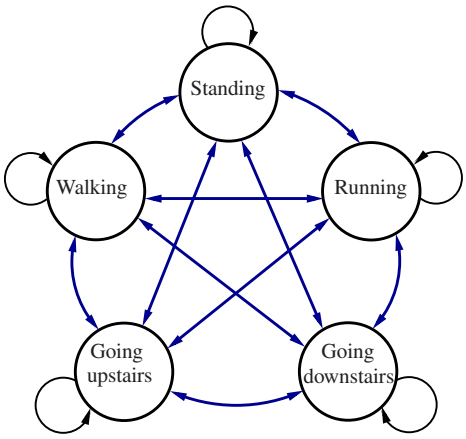

Fig. 5: Architecture of the considered HMM for activity classification.

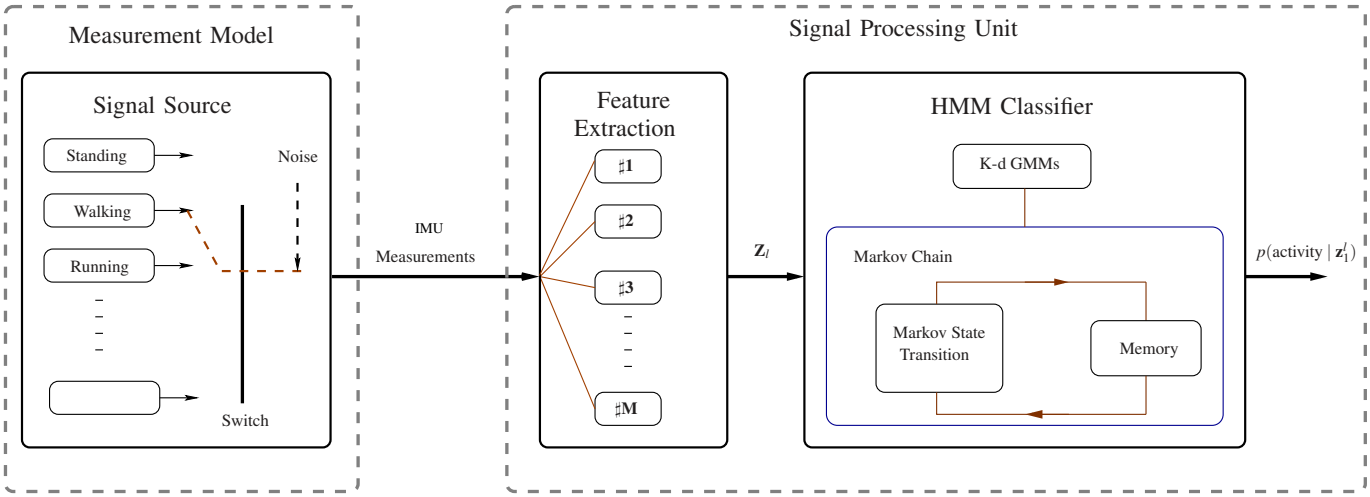

Fig. 6: Schematic representation of the developed system. The signal source block models the pedestrian activity behavior using a switch structure. In the proposed solution a proper feature vector is first extracted from the IMU measurements, and then an HMM-based classifier is applied to find the posterior probability of each of the possible activity classes.

which has five states corresponding to five different activity classes is applied to classify the obtained feature vectors (Fig. 5). The components of the HMM classifiers are schematically illustrated in Fig. 6. In this figure an internal source category (standing, walking, ...) generates a signal and the goal is to recognize the signal source in the classifier. Noise can be added to the system at several points. Feature vector $\mathbf{Z}_l$ is obtained in the feature extraction part and is passed to the classifier. The HMM classifier consists of two objects: a discrete first order Markov chain and the probability density functions of the feature vectors that are considered to be GMMs in this paper. To deal with the previously mentioned measurement noise and IMU displacement variation, feature vectors are modeled with continuous GMMs as:

$$f_{\mathbf{Z}_l|S_l}(\mathbf{z}_l \mid S_l = i) = \sum_{m=1}^{M} w_{m,i} \mathcal{N}(\mathbf{z}_l; \mu_{m,i}, C_{m,i}), \tag{3}$$

where $\mathcal{N}(\mathbf{z}_l; \mu_{m,i}, C_{m,i})$ represents a multivariate Gaussian distribution with mean vector $\mu_{m,i}$ and covariance matrix

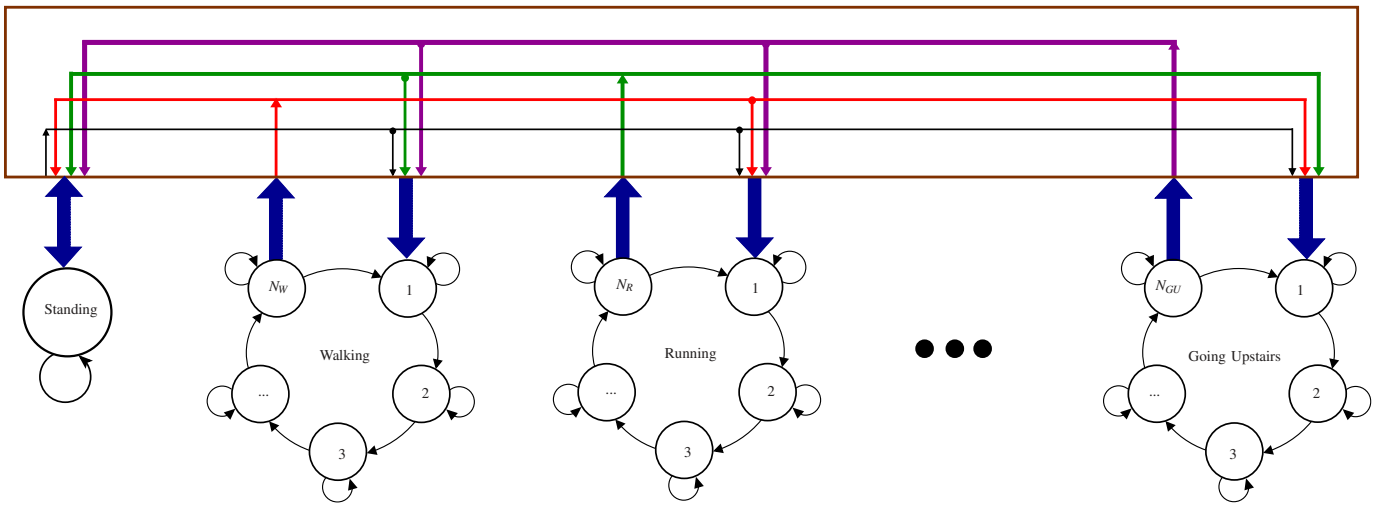

Fig. 7: Architecture of the circular HMM with the corresponding sub-HMMs for different activities. All the sub-HMMs are connected together to design a single HMM that models pedestrian activity.

$C_{m,i}$. Moreover, $\sum_{m=1}^{M} w_{m,i} = 1$. In the experiments, we set empirically $M = 3$, and the covariance matrices were restricted to be diagonal. While the correlations between different features are captured by using the mixture distribution, the assumption of diagonal covariance matrices reduces the number of the unknown parameters that must be estimated, which is beneficial in dealing with low amount of training data. As a result, the considered HMM is characterized by the parameters of the Markov chain $\{A, q\}$ and the parameters of the state-conditional output probability density functions, i.e., parameters of the GMMs $\{\mu, C, w\}$. The transition matrix of the Markov chain, A, models the slow changes in the type of the activity and its elements are defined as $a_{i,j} = p(S_{l+1} = j \mid S_l = i)$ where S_l denotes the activity type in time-frame l and is referred to as the hidden state. The vector q is the initial state probability mass function with $q_j = p(S_1 = j)$. In the current model, it makes sense to predefine A and q based on some sensible values of the tendency of humans to switch between different activity types; therefore, we set

$$q \in \mathbb{R}^{5\times 1}_{\geq 0}, \quad q_j = \begin{cases} 1 & \text{for } j = 5 \quad \text{(Standing)} \\ 0 & \text{for } j \neq 5 \end{cases} \qquad \text{and} \qquad A \in \mathbb{R}^{5\times 5}_{\geq 0}, \quad a_{i,j} = \begin{cases} 0.9 & \text{for } i = j \\ 0.025 & \text{for } i \neq j \end{cases}.$$

The estimation of the GMM parameters is done using an expectation maximization (EM) algorithm [42], [43]. In the test phase, the classification is done by applying the forward algorithm [44] to find the probability for each of the aforementioned states given all the current and previous measurements from the IMU, i.e., $p_{S_l|\mathbf{z}_1^l}\left(S_l = i \mid \mathbf{z}_1^l\right)$, where $\mathbf{z}_1^l$ denotes the feature vectors measured from time-frame 1 till l, i.e., $\mathbf{z}_1^l = \{\mathbf{z}_1, \ldots \mathbf{z}_l\}$. The most probable state can be considered as the output of the classification procedure.

2) Joint Activity Classification and Gait Analysis: For this problem, a classification algorithm is developed that simultaneously classifies the pedestrian activity and the gait-phase of each gait cycle, i.e., a sub-state of the

pedestrian activity. Similar to Subsection III-B1, the pedestrian activity is modeled with a continuous HMM. But, each gait cycle of the IMU signals which corresponds to one step is further modeled with a smaller circular HMM. In this case, each state of these circular HMMs corresponds to one gait-phase. This is motivated by the fact that the IMU signals reveal cyclical patterns for most of the pedestrian activities. In other words, different HMMs, conditioned on a specific activity-type, are forced to have a circular structure whenever it is appropriate. In the following, these circular HMMs are referred to as sub-HMMs. The higher layer HMM, which models the human activity, is obtained by combining all of the circular HMMs. The explained circular HMMs are left-to-right HMMs (where only transitions from one state to the next state is allowed) with an additional property that the last state is connected to the first state; Fig. 7 demonstrates the structure of the designed sub-HMMs and their integrations to create the higher-layer HMM. In this case, a different number of states should be considered for the sub-HMMs depending on the activity type. In our experiments, we trained 4 states for all the activity classes except standing which was modeled by a single state.

In a similar vein to Subsection III-B1, instead of the raw IMU measurements, feature vectors are obtained and are fed into the HMMs. For this purpose, the IMU signals are segmented and windowed into overlapped short-time frames. The signal windowing was done using a frame length of 20 samples with 75% overlap. In this paper, four features are computed for each given short-time frame. These include 1) mean, 2) variance, 3) slope, and 4) curvature; a second-order polynomial was fitted to the data in each segment, and the slope and curvature were calculated by taking the first and second derivatives of the signal, respectively. The final feature vector is then constructed by concatenating all the feature vectors for each of the IMU output signals. As before, the distribution of the feature vectors is assumed to be GMM. For the implementation, two Gaussian components were considered for each state of the sub-HMMs and both were restricted to have diagonal covariance matrices.

Each circular sub-HMM is identified by its Markov chain parameters $\{A,q\}$ and GMM parameters $\{\mu,C,w\}$, as given in (3). The transition matrix for an N-state circular sub-HMM will look like this:

$$A=\begin{bmatrix} a_{11} & a_{12} & 0 & \dots & 0 \\ 0 & a_{22} & a_{23} & \dots & 0 \\ \vdots & \vdots & \ddots & \ddots & \vdots \\ 0 & 0 & \dots & a_{N-1,N-1} & a_{N-1,N} \\ a_{N,1} & 0 & \dots & 0 & a_{N,N} \end{bmatrix}.$$

Given the training data for different pedestrian activities, the parameters of different sub-HMMs are estimated using the Baum-Welch algorithm [42], [44], which is an EM algorithm, to obtain Maximum Likelihood (ML) estimates of the desired parameters. Then, to obtain the general HMM for describing the pedestrian activity, all the sub-HMMs are combined together. Hence, the number of the states for this HMM is equal to the sum of the

number of the states for all the sub-HMMs. For this HMM, all the elements of the initial state probability vector corresponding to the first state of the sub-HMMs are set to have the same value (equiprobable states). Also, the state-conditional output distribution functions are taken from the sub-HMMs. After putting the transition matrices of the sub-HMMs at the proper positions in the transition matrix, some small heuristic transition probabilities are set to allow transitions from the last state of each sub-HMM to the first state of all the other sub-HMMs. Finally all the rows are normalized to create a valid transition probability matrix.

After the training, the classification is done by applying the forward algorithm [44], similarly to Subsection III-B1, to find the probability for each of the aforementioned sub-states given all the current and previous measurements from the IMU, i.e., $p_{S_l|\mathbf{z}_1^l}\left(S_l = i \mid \mathbf{z}_1^l\right)$ where S_l denotes the hidden state in short-time frame l, i.e., S_l corresponds to a specific gait-phase from a particular activity type. As a result, the most probable state can be used to infer the gait-phase and the activity-type simultaneously.

In general, any state from a circular HMM can be considered as the initial state, therefore a circular HMM does not require any reference point in the input signals for training and testing. However, if the defined initial and final states are supposed to correspond to specific gait-phases, it is important to initialize the GMM components in a clever way, e.g., by segmenting each cycle of the IMU output signals into equal parts, then, the first segments of each of the signals' cycles are used to initialize the parameters of the first state. In the current application, it makes sense to consider the first and last states as the beginning and the end of one step. Then, different phases of human gait can be inferred by looking at the corresponding state. Fig. 8d shows an example; this figure shows the first IMU output signal (a_x) together with the classified states for walking and running. As it is shown, state indices 4 and 8 correspond to the zero-crossing phases of their corresponding activity-types, walking and running respectively.

IV. Experiments

The main contribution of this work is the proposed probabilistic, user-independent classification methods for the specifically defined setup, i.e., Chem-IMU, which facilitates the application of this setup in different areas such as vision-aided inertial navigation. The performance of the proposed algorithms is analyzed both qualitatively and quantitatively in this section.

A. Subject Selection

In order to obtain a sufficient amount of data for training, ten subjects–three females and seven males–participated in the experiment; TABLE I summarizes both the train-set and test-set subjects' personal characteristics. All the participants were healthy researchers, without any abnormality in their gait cycles, at the Signal Processing Lab and Communication Theory Lab at KTH. None of the train-set subjects were included in the test-set during the

TABLE I: Train-set and test-set subjects' personal characteristics.

	Number of subjects	Height	Weight	Age
Train	10	174±12	68.7±12.5	29.5±4
Test	4	175±11	74.5±12	30±4.9

TABLE II: Approximate cumulative length of the test signals.

		Walking	Running	Going upstairs	Going downstairs	Standing
	Recorded data (min)	12	3.4	2.5	2.5	3
Number of decision	Activity classification	1440	408	300	300	360
	Joint activity and gait-phase classification	1440	816	300	300	720

evaluation process. Similar patterns were observed in the IMU measurements independently of its position on the chest (affecting the DC level of the signals). TABLE II provides the approximate cumulative length of the test signals for all the considered classes. Moreover, the approximate length of the recorded activities for the training phase is: walking = 25 min, running = 3 min, going upstairs = 2.5 min, going downstairs = 2.5 min, and standing = 3 min.

B. Performance Evaluation

For presentation purposes, the DC levels of the IMU signals are removed in the following figures. TABLE III shows the corresponding state indices for different activities in both the first and second proposed methods. The performance of the proposed classification approaches is demonstrated in Fig. 8 for different combinations of the activities. The figure presents the first IMU output signal, which corresponds to the orthogonal acceleration, a_x. The results of the classification methods are also plotted over the same signal with red color. The top panel shows the results of the first proposed method and the bottom panel shows the results of the joint activity and gait-phase classification, the second proposed method. Fig. 8a and Fig. 8d illustrate the orthogonal acceleration signal of the IMU when the user moves from standing to walking and finishes running. Respectively, Fig. 8b and Fig. 8e represent the sequence of standing $\rightarrow$ walking $\rightarrow$ going downstairs. Finally, Fig. 8c and Fig. 8f show the sequence of standing $\rightarrow$ walking $\rightarrow$ going upstairs. Comparing the states' numbers in these figures with TABLE III verifies that both of the proposed methods have recognized the underlying activity-type correctly. It is also interesting to notice how the duration of the gait-phase states (bottom panel Fig. 8d, Fig. 8e, and Fig. 8f) vary in different scenarios within each activity class. A simple example of this behavior can be seen in Fig. 8d; during the transition from walking to running, between samples 1000 and 1200, when the underlying signal does not fit either the walking or running states properly, the state index 4 (last state of the walking) is prolonged unusually until the signal can be explained reasonably well by the running model, then, the activity is classified as running by transiting from state index 4 to state index 5 (the first state of running).

The evaluations show that most wrong classifications happen during transitions between activities. To demonstrate this phenomenon, the IMU measurements were continuously recorded for a set of activities. Fig. 9 presents the 6

TABLE III: Considered classes of the activities and corresponding state indices in the trained models.

	Walking	Running	Going upstairs	Going downstairs	Standing
Activity classification	1	2	3	4	5
Joint activity and gait-phase classification	1→4	5→8	9→12	13→16	17

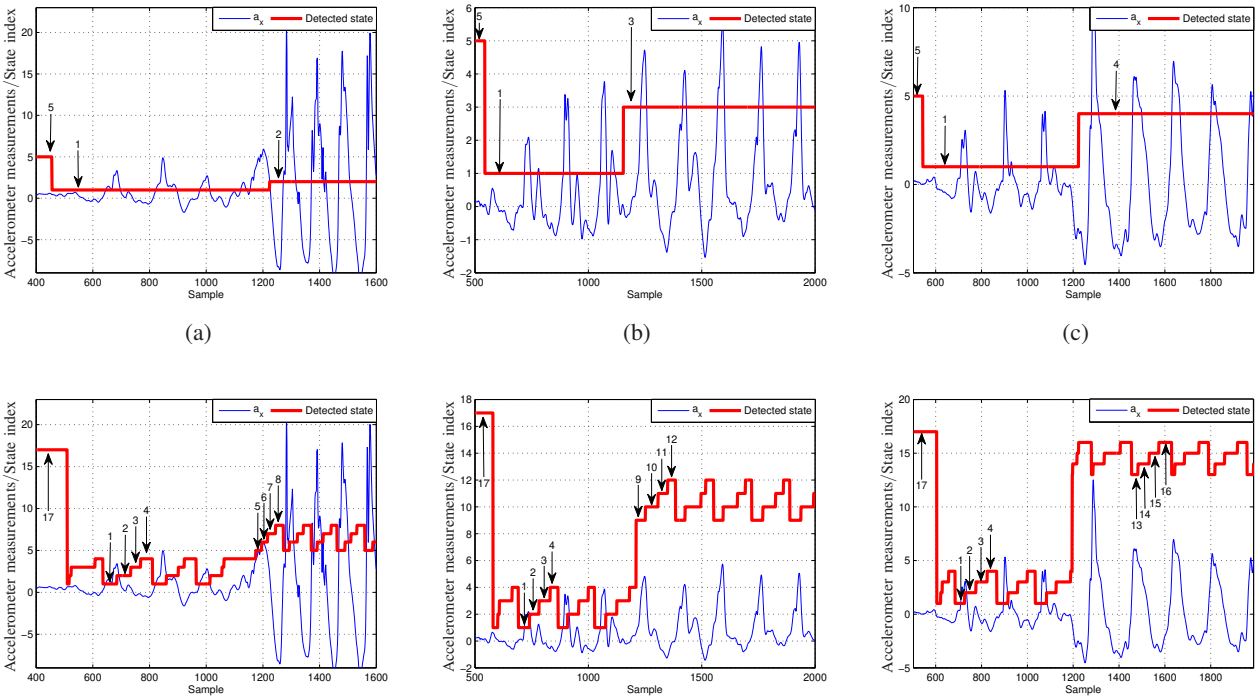

Fig. 8: First IMU output signal (a_x), for the defined activity classes along with the classified activities in subfigure (a), (b), and (c), and the classified joint activity and gait-phases in subfigure (d), (e), and (f). The classified activity and gait-phases are labeled by their corresponding state indices as described in TABLE III.

IMU measurements; three acceleration $[a_x, a_y, a_z]$ signals are plotted in the top panel where three angular rotations $[\omega_x, \omega_y, \omega_z]$ are plotted in the bottom panel. For the sake of visibility, the normalized IMU measurements are shifted along the y axes. The signals present the following activities: standing → walking → standing → running → standing → going downstairs → standing → going upstairs → standing. During the standing periods, the subject was asked to turn around without changing his position, this type of turning around is mostly visible in the gyroscope measurements and is included in the standing state as mentioned before.

For this example, the classified activities and gait-phases are plotted over the first IMU output signal, a_x, in Fig. 10 and Fig. 11 respectively. For clarity, some important segments of Fig. 11 are zoomed and plotted in the bottom panel of the same figure. As can be seen in the figures, almost the same types of mis-classification happen using both of the developed methods during the transitions. Incorrect classifications during transitions mainly occur because of the body configuration switching from one activity-type to another. Therefore, the IMU measurements cannot be modeled with either the preceding or the following activity-type well enough. As a result, the system is

TABLE IV: Confusion matrix, activity classification using the first proposed method, III-B1.

		Classified activity				
		Walking	Running	Going upstairs	Going downstairs	Standing
Actual activity	Walking	90%	0%	5%	5%	0%
	Running	0%	96%	2.7%	1.3%	0%
	Going upstairs	6%	0%	91%	3%	0%
	Going downstairs	6%	0%	4%	90%	0%
	Standing	0%	0%	1%	1%	98%

TABLE V: Confusion matrix, activity classification using the second proposed method, III-B2.

		Classified activity				
		Walking	Running	Going upstairs	Going downstairs	Standing
Actual activity	Walking	97.5%	0%	2%	0.5%	0%
	Running	0.5%	98.5%	1%	0%	0%
	Going upstairs	2.5%	0%	90%	7.5%	0%
	Going downstairs	1%	1%	2%	96%	0%
	Standing	0.5%	0%	0.3%	0.2%	99%

mistakenly recognizes the underlying activity-type.

To evaluate the correct activity classification rate of the proposed methods, a supervised classification was performed for which all the data was labeled manually. For this purpose, all the test-set subjects (TABLE I) were asked to perform natural activities including standing, walking, running, going downstairs, and going upstairs in an indoor environment and with frequent transitions between the activities.

The correct activity classification rate averaged over all the test-set subjects are reported in TABLE IV and TABLE V for the first proposed method and the second proposed method, respectively. The results are reported in the form of a confusion matrix. Each column of this matrix represents the instances from the classified classes, while each row represents the instances from the actual classes. Hence, the diagonal cells of the tables report the correct classification rate for the corresponding activity. The achieved results for both of the proposed algorithms indicate a promising performance; a rate of about 95% correct classification (with marginally better performance for the second method). Even though, this rate is good enough for the desired applications, it should be highlighted that under the stationary conditions (when the subject does not change his/her activity type rapidly), the correct classification rate would be even higher. This is because most incorrect classifications took place during the switching time between activities, and in our test set, subjects were asked to switch between different activities more frequently than in a daily-life scenario. Thus, the reported classification rate is a pessimistic bound on the achievable result.

V. Discussion

The main idea of this study was to devise an IMU setup that could potentially be used in vision-aided navigation systems and to present a method for both activity classification and joint activity and gait-phase classification. We proposed chest mounting the IMU and showed how the IMU signals for the Chem-IMU reveal cyclical patterns as dose the lower-body positioned IMU (Fig. 3). Then, two HMM-based classifiers were introduced for

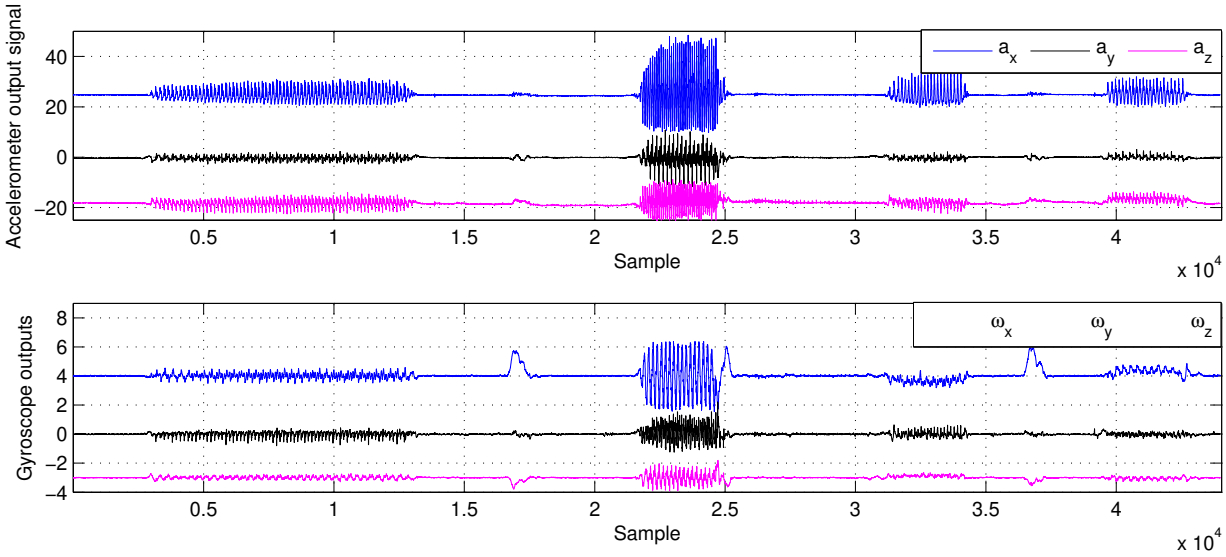

Fig. 9: IMU measurements, accelerometers and gyroscopes, for all the five defined states. For the sake of the visibility, signals are shifted over the y axes. The signals correspond to the following activities: standing → walking → standing → running → standing → going upstairs → standing → going downstairs → standing.

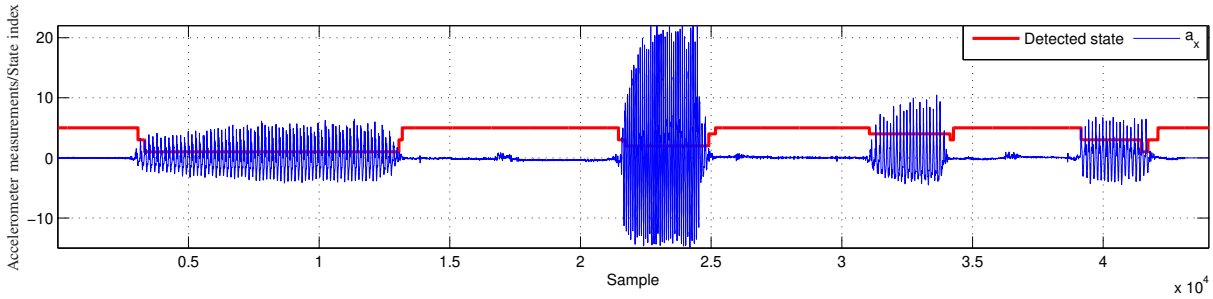

Fig. 10: First IMU output signal (a_x), for all the five defined motion states together with the classified activities based on the first method, III-B1 (see TABLE III for the state indices). The corresponding IMU measurements are plotted in Fig. 9.

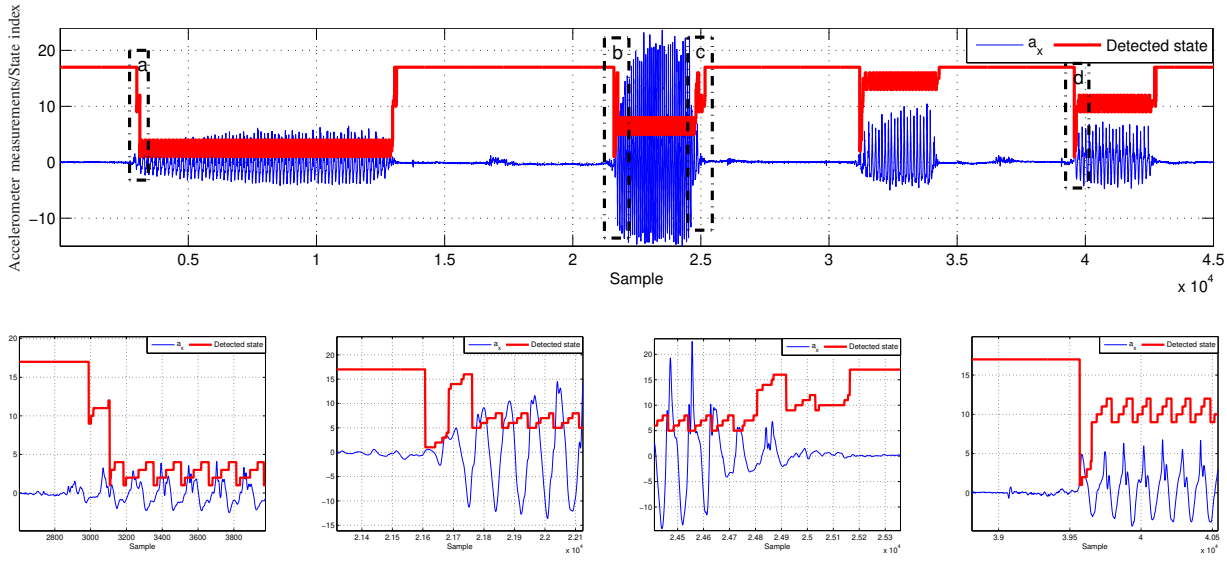

(a) (b) (c) (d)

Fig. 11: First IMU output signal (a_x), for all the five defined motion states together with the classified gait-phase based on the second method, III-B1(see TABLE III for the state indices). The corresponding IMU measurements are plotted in Fig. 9. Subfigure (a)-(d) illustrate the magnified demonstration of the specified parts of the signal with the corresponding box name.

the two aforementioned problems. Since no alternative solution is presented for this problem in the literature, the performances of the proposed algorithms were self-analyzed and compared both qualitatively and quantitatively. The conducted experiments with both of the classifiers showed a high probability of correct activity classification (around 95%). Thus, in addition to being a more suitable choice for the vision-aided navigation systems [1], [21], [45], Chem-IMU can be reliably used for both activity classification and gait analysis.

Although the two proposed methods are different in the feature extraction and exploited HMM structure, similar levels of accuracies were found for both of the provided methods with a marginally better correct performance obtained using the joint activity and gait-phase classification (TABLE IV and V). However, the main advantage of the latter scheme is the provision of gait analysis. For example, one interesting application of this probabilistic method is in step detection. In addition to the classic step detection approaches that cannot cover different walking patterns or irregular motions [26], [46], probabilistic methods can provide higher detection accuracy [24], [25]. Moreover, the delay in the output of the classification and the computational complexity are lower for the second proposed method. This is a consequence of the chosen time-frame length for DFT analysis in the first method.

Considering the performance of state-of-the-art activity classification methods (a correct classification rate between 85% and 99% [24], [30], [36], [40]), the achieved results imply that the Chem-IMU can be used for human activity classification with state-of-the-art performance. However, these methods are mainly developed for foot-mounted IMU and, if desired, in applying those to the Chem-IMU special considerations might be required. Nevertheless, a comprehensive study comparing the Chem-IMU (upper-body positioned IMU) and foot-mounted IMU (lower-body positioned IMU), similar to [40], would be very informative and interesting, but beyond the scope of the current study.

In our paper, we developed probabilistic activity classification methods that can be trained by a set of supervised subjects and activity scenarios. In contrast to the threshold-based [30], [31] and fuzzy logic methods [8], our HMM-based solutions can be easily applied to classify the measurements from new subjects with no further supervision.

There are a number of limitations to this study. First, subjects were asked to physically carry the acquisition device (a laptop connected to the IMU) with them; this might have forced them to change their normal movement slightly. Nevertheless, due to the probabilistic model of the measurements, it is expected that the performance in a normal life scenario remains close to the reported results. One additional weakness of the joint activity classification and gait analysis could be that the feature extraction is done in an ad-hoc manner. A further study with more focus on feature extraction for this approach is therefore suggested.

VI. Conclusion

Low-complexity and accurate human activity monitoring is an important task both in navigation and biomedical applications. In this paper, a setup has been proposed for pedestrian activity classification and gait analysis using

the measurements from a chest-mounted IMU (Chem-IMU). As the classification method, the continuous HMM with GMM output density functions has been used to classify the pedestrian activities. The additional gait-phase analysis is useful in health care and clinical applications to study the duration of each gait cycle and the step pattern of individuals. Moreover, the provided step information, the step number, together with the classified activity-type can be used to estimate the travel distance and dead reckoning for navigational purposes. The performance of the proposed methods has been evaluated by experimental data using the trained HMMs. The probability of the correct classification rate, based on our experiments, was about 0.95, with marginally better performance for the joint activity and gait classification method. This performance rate is comparable with the current state-of-the-art and is good enough for different applications, e.g., as an interesting future investigative direction for visual-inertial navigation systems.

ACKNOWLEDGMENT

The authors would like to thank all the participants in the Signal Processing Lab and Communication Theory Lab at KTH, who kindly helped us in data collection. Parts of this work have been funded by The Swedish Agency for Innovation Systems (VINNOVA).

REFERENCES

[1] R. Jirawimut, S. Prakoonwit, F. Cecelja, and W. Balachandran, "Visual odometer for pedestrian navigation," *IEEE Transactions on Instrumentation and Measurement*, vol. 52, pp. 1166–1173, Aug. 2003.

[2] C.-W. Tan and S. Park, "Design of accelerometer-based inertial navigation systems," *IEEE Transactions on Instrumentation and Measurement*, vol. 54, pp. 2520–2530, Dec. 2005.

[3] M. Adams, W. Wijesoma, and A. Shacklock, "Autonomous navigation: Achievements in complex environments," *IEEE Instrumentation Measurement Magazine*, vol. 10, pp. 15–21, Jun. 2007.

[4] P. Händel, "Discounted least-squares gearshift detection using accelerometer data," *IEEE Transactions on Instrumentation and Measurement*, vol. 58, pp. 3953–3958, Dec. 2009.

[5] P. Händel, B. Enstedt, and M. Ohlsson, "Combating the effect of chassis squat in vehicle performance calculations by accelerometer measurements," *Measurement*, vol. 43, no. 4, pp. 483–488, 2010.

[6] P. Szemes, H. Hashimoto, and P. Korondi, "Pedestrian-behavior-based mobile agent control in intelligent space," *IEEE Transactions on Instrumentation and Measurement*, vol. 54, pp. 2250–2257, Dec. 2005.

[7] A. Sabatini, C. Martelloni, S. Scapellato, and F. Cavallo, "Assessment of walking features from foot inertial sensing," *IEEE Transactions on Biomedical Engineering*, vol. 52, pp. 486–494, Mar. 2005.

[8] C. Senanayake and S. Senanayake, "Computational intelligent gait-phase detection system to identify pathological gait," *IEEE Transactions on Information Technology in Biomedicine*, vol. 14, pp. 1173–1179, Sep. 2010.

[9] K. Aminian and B. Najafi, "Capturing human motion using body-fixed sensors: outdoor measurement and clinical applications," *Computer Animation and Virtual Worlds*, vol. 15, no. 2, pp. 79–94, 2004.

[10] W. Wan, H. Liu, L. Wang, G. Shi, and W. Li, "A hybrid HMM/SVM classifier for motion recognition using μIMU data," in *IEEE Int. Conf. on Robotics and Biomimetics*, pp. 115–120, Dec. 2007.

[11] C. C. Yang and Y. L. Hsu, "A review of accelerometry-based wearable motion detectors for physical activity monitoring," *Sensors*, vol. 10, no. 8, pp. 7772–7788, 2010.

[12] A. Akl, C. Feng, and S. Valaee, "A novel accelerometer–based gesture recognition system," *IEEE Transactions on Signal Processing*, vol. 59, pp. 6197–6205, Dec. 2011.

[13] H. Vathsangam, A. Emken, E. Schroeder, D. Spruijt-Metz, and G. Sukhatme, "Determining energy expenditure from treadmill walking using hip-worn inertial sensors: An experimental study," *IEEE Transactions on Biomedical Engineering*, vol. 58, pp. 2804–2815, Oct. 2011.

[14] Ö. Bebek, M. A. Suster, S. Rajgopal, M. J. Fu, X. Huang, M. C. Cavusoglu, D. J. Young, M. Mehregany, A. J. Van Den Bogert, and C. H. Mastrangelo, "Personal navigation via high-resolution gait-corrected inertial measurement units," *IEEE Transactions on Instrumentation and Measurement*, vol. 59, no. 11, pp. 3018–3027, 2010.

[15] G. Panahandeh, I. Skog, and M. Jansson, "Calibration of the accelerometer triad of an inertial measurement unit, maximum likelihood estimation and cramer-rao bound," in *IEEE Int. Conf. on Indoor Positioning and Indoor Navigation IPIN*, Sep. 2010.

[16] A. Jimenez Ruiz, F. Seco Granja, J. Prieto Honorato, and J. Guevara Rosas, "Accurate pedestrian indoor navigation by tightly coupling foot-mounted IMU and RFID measurements," *IEEE Transactions on Instrumentation and Measurement*, vol. 61, pp. 178–189, Jan. 2012.

[17] I. Skog and P. Händel, "In-car positioning and navigation technologies–a survey," *Intelligent Transportation Systems, IEEE Transactions on*, vol. 10, pp. 4–21, Mar. 2009.

[18] J. Fang and X. Gong, "Predictive iterated Kalman filter for INS/GPS integration and its application to SAR motion compensation," *IEEE Transactions on Instrumentation and Measurement*, vol. 59, pp. 909–915, Apr. 2010.

[19] D. Grejner-Brzezinska, C. Toth, H. Sun, X. Wang, and C. Rizos, "A robust solution to high-accuracy geolocation: Quadruple integration of GPS, IMU, pseudolite, and terrestrial laser scanning," *IEEE Transactions on Instrumentation and Measurement*, vol. 60, pp. 3694–3708, Nov. 2011.

[20] N. El-Sheimy, K.-W. Chiang, and A. Noureldin, "The utilization of artificial neural networks for multisensor system integration in navigation and positioning instruments," *IEEE Transactions on Instrumentation and Measurement*, vol. 55, pp. 1606–1615, Oct. 2006.

[21] G. Panahandeh, D. Zachariah, and M. Jansson, "Exploiting ground plane constraints for visual-inertial navigation," in *IEEE-ION Position Location and Navigation Symposium (PLANS)*, 2012.

[22] E. Foxlin, "Pedestrian tracking with shoe-mounted inertial sensors," *IEEE Computer Graphics and Applications*, vol. 25, pp. 38–46, Nov.-Dec. 2005.

[23] J. Rantakokko, J. Rydell, P. Stromback, P. Händel, J. Callmer, D. Tornqvist, F. Gustafsson, M. Jobs, and M. Gruden, "Accurate and reliable soldier and first responder indoor positioning: multisensor systems and cooperative localization," *IEEE Wireless Communications*, vol. 18, pp. 10–18, Apr. 2011.

[24] Z. Sun, X. Mao, W. Tian, and X. Zhang, "Activity classification and dead reckoning for pedestrian navigation with wearable sensors," *Measurement Science and Technology*, vol. 20, no. 1, 2009.

[25] X. Chen, S. Hu, Z. Shao, and J. Tan, "Pedestrian positioning with physical activity classification for indoors," in *IEEE Int. Conf. on Robotics and Automation (ICRA)*, pp. 1311–1316, May. 2011.

[26] L. Fang, P. Antsaklis, L. Montestruque, M. McMickell, M. Lemmon, Y. Sun, H. Fang, I. Koutroulis, M. Haenggi, M. Xie, and X. Xie, "Design of a wireless assisted pedestrian dead reckoning system–the NavMote experience," *IEEE Transactions on Instrumentation and Measurement*, vol. 54, pp. 2342–2358, Dec. 2005.

[27] A. Bourke, J. O'Brien, and G. Lyons, "Evaluation of a threshold-based tri-axial accelerometer fall detection algorithm," *Gait & Posture*, vol. 26, no. 2, pp. 194–199, 2007.

[28] J. Chen, K. Kwong, D. Chang, J. Luk, and R. Bajcsy, "Wearable sensors for reliable fall detection," in *IEEE-EMBS 27th Annual Int. Conf. of the Engineering in Medicine and Biology Society*, pp. 3551–3554, Jan. 2005.

[29] W. Zijlstra and A. L. Hof, "Assessment of spatio–temporal gait parameters from trunk accelerations during human walking," *Gait and Posture*, vol. 18, no. 2, pp. 1–10, 2003.

[30] I. P. I. Pappas, M. R. Popovic, T. Keller, V. Dietz, and M. Morari, "A reliable gait phase detection system," *IEEE Transactions on Neural Systems and Rehabilitation Engineering*, vol. 9, pp. 113–125, Jun. 2001.

[31] B. Smith, D. Coiro, R. Finson, R. Betz, and J. McCarthy, "Evaluation of force-sensing resistors for gait event detection to trigger electrical stimulation to improve walking in the child with cerebral palsy," *IEEE Transactions on Neural Systems and Rehabilitation Engineering*, vol. 10, pp. 22–29, Mar. 2002.

[32] Z. Liu and C.-H. Won, "Knee and waist attached gyroscopes for personal navigation: Comparison of knee, waist and foot attached inertial sensors," in *IEEE/ION Position Location and Navigation Symposium (PLANS)*, pp. 375–381, May. 2010.

[33] G. Panahandeh and M. Jansson, "Vision-aided inertial navigation using planar terrain features," in *IEEE Int. Conf. on Robot, Vision and Signal Processing*, Sep. 2011.

[34] C. Hide, T. Botterill, and M. Andreotti, "Low cost vision-aided IMU for pedestrian navigation," in *Proc. of UPINLBS*, pp. 1–7, Oct. 2010.

[35] S. K. Park and Y. S. Suh, "A zero velocity detection algorithm using inertial sensors for pedestrian navigation systems," *Sensors*, vol. 10, no. 10, pp. 9163–9178, 2010.

[36] G. Shi, Y. Zou, Y. Jin, X. Cui, and W. Li, "Towards HMM based human motion recognition using MEMS inertial sensors," in *IEEE Int. Conf. on Robotics and Biomimetics ROBIO*, pp. 1762–1766, Feb. 2009.

[37] G. Panahandeh, N. Mohammadiha, A. Leijon, and P. Händel, "Chest-mounted inertial measurement unit forpedestrian motion classification using continuous hidden Markov model," in *IEEE Int. Instrumentation and Measurement Technology Conf. (I2MTC)*, pp. 991–995, May. 2012.

[38] M. Chen, B. Huang, and Y. Xu, "Human abnormal gait modeling via hidden Markov model," in *IEEE Int. Conf. on Information Acquisition ICIA*, pp. 517–522, Jul. 2007.

[39] M. Susi, D. Borio, and G. Lachapelle, "Accelerometer signal features and classification algorithms for positioning applications," in *Proceedings of the 2011 Int. Technical Meeting of The Institute of Navigation, San Diego*, January 2011.

[40] S. Preece, J. Goulermas, L. Kenney, and D. Howard, "A comparison of feature extraction methods for the classification of dynamic activities from accelerometer data," *IEEE Transactions on Biomedical Engineering*, vol. 56, pp. 871–879, Mar. 2009.

[41] M. Asgharioskoei and H. Hu, "Myoelectric control systemsa survey," *Biomedical Signal Processing and Control*, vol. 2, no. 4, pp. 275–294, 2007.

[42] J. Bilmes, "A gentle tutorial of the EM algorithm and its application to parameter estimation for Gaussian mixture and hidden Markov models," tech. rep., Univ. California, Berkeley, TR-97-021 Rep, 1997.

[43] A. P. Dempster, N. Laird, and D. B. Rubin, "Maximum likelihood from incomplete data via the EM algorithm," *J. R. Statist. Soc*, vol. 39, no. 1, pp. 1–38, 1977.

[44] L. Rabiner, "A tutorial on hidden Markov models and selected applications in speech recognition," *Proceedings of the IEEE*, vol. 77, pp. 257–286, Feb. 1989.

[45] N. Kyriakoulis and A. Gasteratos, "Color-based monocular visuoinertial 3-d pose estimation of a volant robot," *IEEE Transactions on Instrumentation and Measurement*, vol. 59, pp. 2706–2715, Oct. 2010.

[46] S. Godha, G. Lachapelle, and M. Cannon, "Integrated GPS/INS system for pedestrian navigation in a signal degraded environment," in *Proc. of the 19th Int. Technical Meeting of the Satellite Division of The Institute of Navigation (ION GNSS)*, Sep. 2006.

Ghazaleh Panahandeh (S'11) received the M.S. degree in electronics engineering from Sharif University of Technology, Tehran, Iran, in 2008. She is currently working towards the Ph.D. degree in telecommunications at the Signal Processing Laboratory, KTH Royal Institute of Technology, Stockholm, Sweden. Her research interests include inertial navigation and positioning, vision-aided inertial navigation, estimation theory, and stochastic signal processing. She is a student member of the IEEE.

Nasser Mohammadiha (S'11) received the M.Sc. degree in electronics engineering from Sharif University of Technology, Tehran, Iran, in 2006. He worked on digital hardware and software design until 2008. He is currently pursuing the Ph.D. degree in the telecommunications in the Sound and Image Processing laboratory, KTH Royal Institute of Technology, Stockholm, Sweden. His research interests include speech processing, mainly speech enhancement, image processing, and statistical signal modeling. He is a student member of the IEEE.

Arne Leijon received the MS degree in engineering physics in 1971, and the PhD degree in information theory in 1989, both from Chalmers University of Technology, Gothenburg, Sweden. He has been a professor of hearing technology at the Sound and Image Processing (SIP) Laboratory at the KTH Royal Institute of Technology, Stockholm, Sweden, since 1994. His main research interest concerns applied signal processing in aids for people with hearing impairment, and methods for individual fitting of these aids, based on psychoacoustic modeling of sensory information transmission and subjective sound quality. He is a member of the IEEE.

Peter Händel (S'88-M'94-SM'98) received the Ph.D. degree from Uppsala University, Uppsala, Sweden, in 1993. From 1987 to 1993, he was with Uppsala University. From 1993 to 1997, he was with Ericsson AB, Kista, Sweden. From 1996 to 1997, he was also with the Tampere University of Technology, Tampere, Finland. Since 1997, he has been with the Royal Institute of Technology, Stockholm, Sweden, where he is currently a Professor of Signal Processing. From 2000 to 2006, he worked part time with the Swedish Defence Research Agency. In 2010, he spent some time at the Indian Institute of Science (IISc), Bangalore, as Guest Professor. He is currently a Guest Professor with the University of Gävle, Gävle, Sweden. Dr. Händel has served as an associate editor for the IEEE TRANSACTIONS ON SIGNAL PROCESSING.